

Many-body treatment of hot-electron scattering from quasiequilibrium electron-hole plasmas and coupled plasmon–longitudinal-optic-phonon modes in GaAs

Jeff F. Young and Paul J. Kelly

Institute for Microstructural Sciences, National Research Council, Ottawa, Ontario, Canada K1A 0R6

(Received 28 July 1992)

The interaction of hot electrons (200–300 meV) with neutral electron-hole plasmas in bulk GaAs is theoretically investigated over a range of plasma temperatures and densities. Results obtained using a self-consistent, three-band (electron, heavy-, and light-hole) random-phase approximation for the system's dielectric function, including the lattice susceptibility, are compared with simpler approximations for treating the screened interaction between the hot electrons and the coupled plasma–longitudinal-optic-phonon system. Emphasis is placed on estimating the relative importance of hot-electron plasma versus hot-electron–LO-phonon scattering rates, to the extent that these can be distinguished. The relevance of single-parameter descriptions of the hot-electron “scattering-rate,” such as the total scattering rate out of a well-defined momentum state versus the average energy-loss rate of the hot electron, is discussed; there, specific reference is made to a more complete simulation of experimentally determined hot-electron-plasma scattering rates based only on the *differential* scattering rate. The importance of including the inter-heavy-light-hole polarizability in the system's dielectric-response function is explicitly demonstrated, and scaling parameters are derived that allow simple estimates of the ratio of the hot electron's energy that is coupled to the system via the electron, versus the hole components of the plasma.

I. INTRODUCTION

It is known¹ that free electrons with kinetic energies larger than a longitudinal-optic (LO) -phonon energy (~ 36 meV) in the Γ valley of GaAs scatter to unoccupied, lower-energy states via the emission of LO phonons at a rate of ~ 5 ps⁻¹. This is the dominant relaxation process provided that (i) the kinetic energy of these hot electrons is less than the threshold energy for intervalley scattering to the L (~ 300 meV) or X (~ 500 meV) satellite valleys and (ii) the density of free carriers in the semiconductor is low. After considerable work on the subject and a period of controversy, there now also appears to be general agreement on the absolute rates of intervalley (Γ - L and Γ - X) scattering, which dominate over intra- Γ -valley LO-phonon scattering when allowed.²

However, less is known about the role of carrier-carrier scattering, due at least partly to the many-body nature of the problem. This paper reports the results of a quantitative investigation into the role that a background population of free electrons and holes plays in modifying the scattering and energy-loss rates of hot electrons below the intervalley scattering threshold in GaAs. In particular, the interaction rate of a hot electron with the coupled LO-phonon–neutral-plasma system is calculated self-consistently using both static and full dynamic [exact within the random-phase approximation (RPA)] treatments of the many-body screening processes. Other calculations of hot-electron–plasma scattering rates in bulk GaAs that include dynamic screening have been reported,^{3–6} but to the best of our knowledge, there have been no such treatments that simultaneously include electrons and both heavy- and light-hole valence bands (including the inter-valence-band polarizability). A calculation of

the spectral density function for the two-band, heavy- and light-hole system has been reported,⁶ and the present work incorporates this together with the electron system in a calculation of the differential scattering rate of hot electrons. Preliminary results of part of this work have been reported previously;^{7–9} here we present a complete analysis, emphasizing the underlying physics and applying this knowledge to draw quite general quantitative conclusions whereby practitioners may estimate the effects of background plasmas without the need for detailed calculations.

II. THE MODEL

The model used for the purposes of calculation consists of a single hot test electron in momentum state \mathbf{k} of the Γ conduction band that is assumed to be distinguishable from a background plasma of density N_e electrons, N_h heavy holes, and N_l light holes, where $N_h + N_l = N_e$. The temperature T of all three plasma components and the lattice are taken to be the same. Under these conditions, the differential scattering rate of the test electron undergoing a change in energy $\hbar\omega$ and momentum $\hbar\mathbf{q}$ is $\partial^2\Gamma(\mathbf{k})/\partial\omega\partial\mathbf{q}$. One can conceptually think of the test electron as part of a monochromatic beam, and the differential scattering rate as a measure of the spectrum of electrons scattered from the beam via interactions with the coupled plasma-lattice system. Within the Born approximation, the differential scattering rate can be expressed in terms of the imaginary part of the inverse longitudinal dielectric-response function of the plasma-lattice system, $\text{Im}[1/\epsilon(\omega, \mathbf{q})]$, as^{10,11}

$$\frac{\partial^2\Gamma(\mathbf{k})}{\partial\omega\partial\mathbf{q}} = \frac{2e^2m_e}{\pi\hbar^2kq} \frac{1}{e^{-\beta\hbar\omega} - 1} \text{Im} \left[\frac{1}{\epsilon(\omega, \mathbf{q})} \right], \quad (1)$$

where m_e is the electron effective mass in the conduction band and $\beta=1/k_B T$, where k_B is Boltzmann's constant.

The function $\epsilon(\omega, \mathbf{q})$ can be expressed in terms of the polarizability of the free-carrier system, $P(\omega, \mathbf{q})$; the optical-phonon contribution

$$\epsilon_L(\omega) = (\epsilon_0 - \epsilon_\infty) / (1 - \omega^2 / \omega_T^2),$$

where ω_T is the transverse optic-phonon frequency; and the bare Coulomb interaction $V(q) = 4\pi e^2 / q^2$ as

$$\epsilon(\omega, \mathbf{q}) = \epsilon_\infty + \epsilon_L - V(q)P(\omega, \mathbf{q}), \quad (2)$$

where ϵ_0 (ϵ_∞) is the low- (high-) frequency limit of the background dielectric-response function.

$P(\omega, \mathbf{q})$ must be approximated due to its many-body nature. Different levels of approximation exist, but the most complicated expression used here is that obtained within the random-phase approximation:¹²

$$P(\omega, \mathbf{q}) = \sum_{\mathbf{k}, i, j} \frac{M_{ij}^2(\mathbf{k}, \mathbf{q}) \{f_j(\mathbf{k}) - f_i(\mathbf{k} + \mathbf{q})\}}{\hbar\omega + E_j(\mathbf{k}) - E_i(\mathbf{k} + \mathbf{q}) - i\delta}. \quad (3)$$

Here, $f_i(\mathbf{k})$ represents the Fermi-Dirac occupation factor for *electrons* and $E_i(\mathbf{k})$ the energy of an electron state \mathbf{k} in the i th band. The M_{ij}^2 represent the squared matrix element of $\exp(i\mathbf{q}\cdot\mathbf{r})$ between the Bloch states \mathbf{k} in the j th band and $\mathbf{k} + \mathbf{q}$ in the i th band. The largest characteristic energy scale for the hot-electron scattering process is either the LO-phonon or the plasmon energy. For the carrier densities used here, the plasmon energy is always much less than the kinetic energy of the hot electron, $E(\mathbf{k}) \leq 300$ meV. The energy denominator in the electronic polarizability term therefore discriminates against all interband processes except those separated by $\lesssim 300$ meV. In principle, for GaAs, inter-heavy-light-hole and inter-heavy- or light-split-off hole terms could be included. However, since the split-off band's energy offset is at

the extreme range of this energy scale and since it offers a relatively low density of final states, only the heavy-light-hole interband term was retained in the present calculations. With these simplifications the dielectric-response function becomes

$$\begin{aligned} \epsilon(\omega, \mathbf{q}) = & \epsilon_\infty + \epsilon_L - V(q) \{ P_{ee}(\omega, \mathbf{q}) + P_{hh}(\omega, \mathbf{q}) \\ & + P_{ll}(\omega, \mathbf{q}) + P_{hl}(\omega, \mathbf{q}) \\ & + P_{lh}(\omega, \mathbf{q}) \}, \end{aligned} \quad (4)$$

where e , h , and l refer to the electron, heavy-hole, and light-hole bands, respectively, and where all of the free-carrier terms can be cast in the form

$$P_{ij}(\omega, \mathbf{q}) = \sum_{\mathbf{k}} \frac{M_{ij}^2(\mathbf{k}, \mathbf{q}) \{f_j(\mathbf{k}) - f_i(\mathbf{k} + \mathbf{q})\}}{\hbar\omega + E_j(\mathbf{k}) - E_i(\mathbf{k} + \mathbf{q}) - i\delta}, \quad (5)$$

with the $f_i(\mathbf{k})$ now referring to the electrons in the conduction band and the heavy or light holes in the respective valence bands. The $E_i(\mathbf{k})$ in Eq. (5) are always kinetic energies taken positive with respect to the respective band edges. Within a four-band (including spin) $\mathbf{k}\cdot\mathbf{p}$ perturbation theory, the lowest-order nontrivial matrix elements are¹³

$$M_{ij}^2(\mathbf{k}, \mathbf{q}) = \begin{cases} 1, & i = j = e \\ \frac{1 + 3 \cos^2 \theta}{4}, & i = j = h \text{ or } l \\ \frac{3 \sin^2 \theta}{4}, & i \neq j, i, j = h \text{ or } l, \end{cases} \quad (6)$$

where θ is the angle between \mathbf{k} and $\mathbf{k} + \mathbf{q}$.

At nonzero temperatures, the $\text{Im}[1/\epsilon(\omega, \mathbf{q})]$ in Eq. (1) can be explicitly expressed in terms of the imaginary parts of the free-carrier polarizabilities, $\text{Im}[P(\omega, \mathbf{q})]$, and the squared magnitude of the total dielectric function as

$$\text{Im} \left[\frac{1}{\epsilon(\omega, \mathbf{q})} \right] = V(q) \left\{ \frac{\text{Im}[P_{ee}(\omega, \mathbf{q})] + \text{Im}[P_{hh}(\omega, \mathbf{q})] + \text{Im}[P_{ll}(\omega, \mathbf{q})] + \text{Im}[P_{hl}(\omega, \mathbf{q})] + \text{Im}[P_{lh}(\omega, \mathbf{q})]}{|\epsilon(\omega, \mathbf{q})|^2} \right\}. \quad (7)$$

Explicit expressions for the imaginary parts of Eq. (5) are given in the Appendix. They are general except that for the holes, the $f_i(\mathbf{k})$ are assumed to be of Maxwell-Boltzmann form. This restricts the maximum density of the plasma that can be studied, but not drastically (to $N \approx 1 \times 10^{19} \text{ cm}^{-3}$ at 300 K). The corresponding real parts of Eq. (5) were obtained using a numerical Kramers-Kronig algorithm.

The usual criterion for the applicability of the RPA is that the plasma must be weakly coupled, i.e., the average potential energy should be much less than the average kinetic energy. For plasma parameters such that the distribution functions are Maxwell-Boltzmann-like, this cri-

terion reduces to

$$\frac{e^2 N^{1/3}}{\epsilon_0 k_B T} < 1. \quad (8)$$

As an example, at 100 K, the criterion is satisfied for densities below $2 \times 10^{17} \text{ cm}^{-3}$. The numerical results presented below are all done for plasma parameters that satisfy this criterion.

The static-screening approximation (SSA) consists of taking the zero-frequency limit of $|\epsilon(\omega, \mathbf{q})|^2$ in Eq. (7). A discussion of the physical interpretation of various terms in Eq. (7) is deferred to Sec. IV.

III. RESULTS

A. The differential scattering rate

Figure 1 illustrates the differential scattering rate (restricted to energy-loss processes only) obtained from Eq. (1) for a 300-meV test electron interacting with a plasma of density $N = 8 \times 10^{16} \text{ cm}^{-3}$ at a temperature $T = 300 \text{ K}$. Figure 1(a) was obtained using the SSA, while Fig. 1(b) was obtained using the RPA. The SSA produces a rather featureless spectrum, reflecting that part of the plasma's single-particle excitation spectrum which overlaps the phase space available to the relaxing hot electron. All of the spectral weight in Fig. 1(a) corresponds to direct hot-electron-free-carrier scattering events, i.e., hot-electron-plasma scattering.

The RPA result in Fig. 1(b) is clearly much different

than the SSA result. At low frequencies, a remnant of the SSA single-particle spectrum can be seen, but it is resonantly enhanced where it overlaps the collective plasmon excitation of the multicomponent plasma. In addition, a sharp feature is observed over a range of wave vectors very near the LO-phonon energy. In the limit of zero plasma density, this part of the spectrum is precisely the differential scattering rate via the bare Fröhlich interaction with LO phonons.¹⁴ Under the conditions of Fig. 1, where the plasmon energy is much less than the LO-phonon energy, there is little coupling between the two, and the low-energy part of the spectrum can be interpreted essentially as dynamically screened hot-electron-plasma scattering, and the portion near the LO-phonon energy as bare LO-phonon scattering. Figure 2 shows the corresponding RPA result for a density

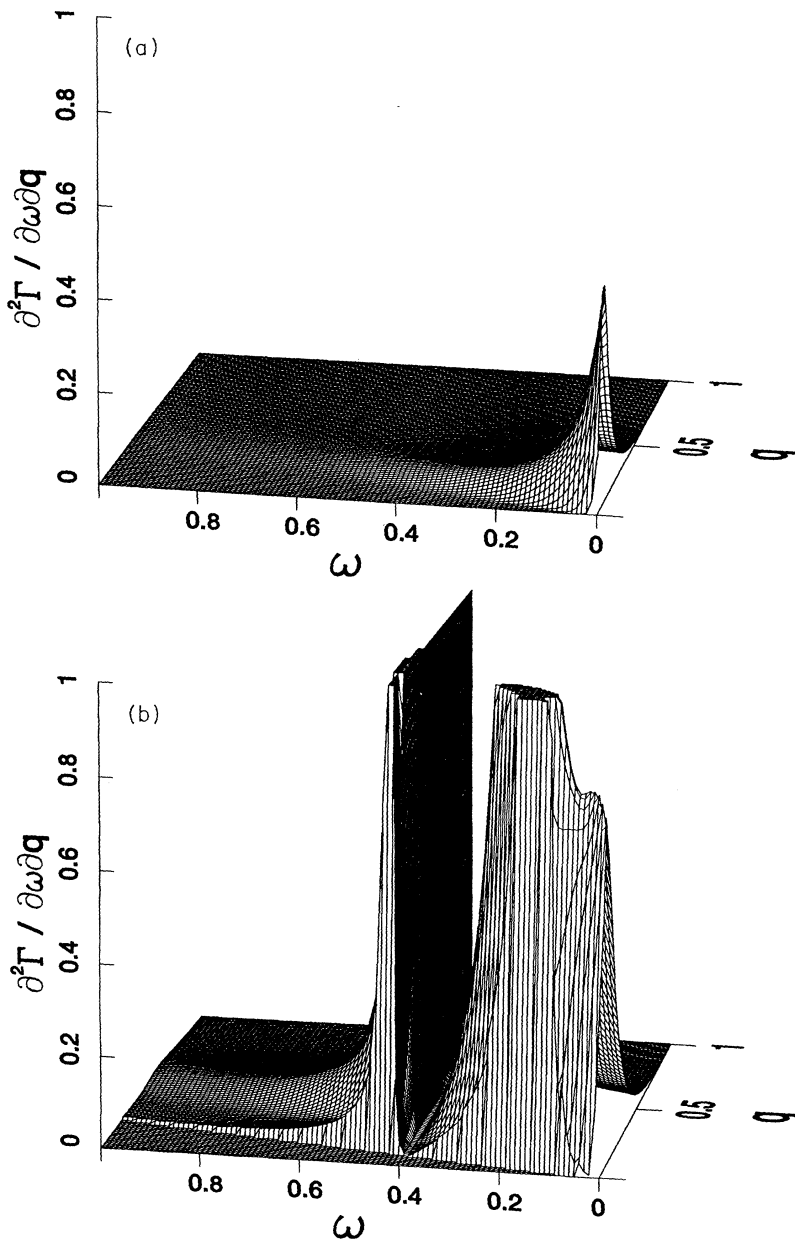


FIG. 1. The total integrand of Eq. (10) for a 300-meV hot electron, a plasma density of $8 \times 10^{16} \text{ cm}^{-3}$, and a temperature of 300 K, calculated (a) using the static-screening approximation and (b) using full dynamic screening, including the lattice susceptibility. Full scale in wave vector corresponds to $7.26 \times 10^6 \text{ cm}^{-1}$, and full scale in frequency corresponds to $1.25 \times 10^{14} \text{ rad/s}$. The integrand has been arbitrarily scaled for presentation.

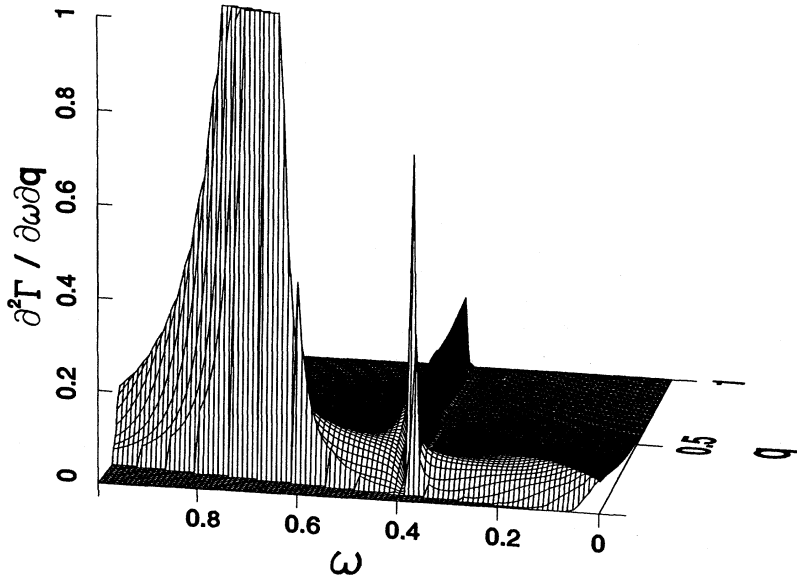


FIG. 2. The total integrand of Eq. (10) for the case of dynamic screening, including the lattice susceptibility for the same parameters as in Fig. 1 but for a plasma density of $1 \times 10^{18} \text{ cm}^{-3}$. Full scale in wave vector corresponds to $7.26 \times 10^6 \text{ cm}^{-1}$, and full scale in frequency corresponds to $1.25 \times 10^{14} \text{ rad/s}$. The vertical scale is the same as in Fig. 1.

of $N = 10^{18} \text{ cm}^{-3}$. Under these conditions the plasmon energy has increased, and the plasma effectively screens out the LO-phonon interaction at small wave vectors, although there remains some spectral weight at the LO-phonon energy for large wave vectors where the plasmon is poorly defined due to strong Landau damping. Under these latter conditions, it is clear from inspection that the hot-electron-plasma scattering dominates the LO-phonon scattering events.

As pointed out in Sec. I, it is of practical interest to estimate under what conditions the hot electron interacts more strongly with the plasma than with the LO phonons that dominate at low carrier densities. To answer this question, it is necessary to be more specific about what is meant by “interacts with.” The differential scattering rate of Eq. (1) can be integrated directly over kinematically allowed phase space to yield the total scattering rate (TSR), equivalent to the inverse quantum lifetime of the state \mathbf{k} . It can also be integrated over the same phase space, but with a multiplicative factor of $\hbar\omega$, to yield the average (in an ensemble sense) energy-loss rate (AELR) of the hot electron. Which of these, if either, are relevant measures of the importance of plasma interactions depends ultimately on comparison with experiments. Different experiments can in principle measure different physical quantities; hence, there may be no single answer to the question posed. In the following, therefore, numerical results for both the AELR and the TSR are presented separately, in Secs. III B and III C, respectively, for a range of plasma and hot-electron parameters. The relevance of these results to potential experiments is discussed. Section III D describes how the differential scattering rates can be combined with a simple Monte Carlo algorithm to simulate accurately an optical pump-probe experiment¹⁵ that, as will be shown, measures an effective hot-electron scattering rate that is a mixture of the TSR and the AELR.

B. The average energy-loss rate

The AELR of the hot electron (in an ensemble sense) is given explicitly by

$$\frac{dE(\mathbf{k})}{dt} = \int_0^\infty dq \int_{-(\hbar q/2m)(2k+q)}^{(\hbar q/2m)(2k-q)} d\omega \hbar\omega \frac{\partial^2 \Gamma(\mathbf{k})}{\partial \omega \partial q} \times [1 - f(\mathbf{k}-\mathbf{q})], \quad (9)$$

where the limits of integration reflect the kinematic restraints on the final state to which the hot electron scatters in the conduction band. When the full dielectric-response function, Eq. (4), is used in evaluating Eq. (9), the resulting AELR self-consistently includes the total interaction with the coupled (and in general indistinguishable) LO-phonon-plasma system. This, of course, is one of the primary motivations for using this self-consistent formalism; however, for the sake of intuitive arguments, it is convenient to attempt a separation of the energy-loss rates via the plasma compared to that via LO phonons. At low densities, $\lesssim 10^{17} \text{ cm}^{-3}$, where the LO-phonon-plasmon coupling is weak [see Fig. 1(b)], such a separation can be attempted with impunity. Numerically, it is easiest to separate the hot-electron-plasma contribution by evaluating Eq. (4) with the lattice contribution, $\epsilon_L(\omega)$ omitted from $\epsilon(\omega, q)$. Figure 3 shows the results of such calculations done for a number of different plasma temperatures and initial hot-electron energies, all as a function of plasma density up to $\sim 10^{17} \text{ cm}^{-3}$.

The results obtained using the full RPA expression for the electronic contributions to $\epsilon(\omega, q)$ are close to linearly dependent on the plasma density and quite insensitive to both the plasma temperature and the initial energy of the hot electron. This is very different from the results for the total scattering rate (see Refs. 3, 4, and 17 and Sec. III B below) which exhibit a strong dependence on plasma temperature and a noticeable dependence on the initial energy of the hot electron.

The AELR results obtained using the SSA exhibit a strong sublinear density dependence, and the absolute values are substantially lower than those obtained from the RPA results. The discrepancy between the dynamic and static results can be qualitatively understood by arguing that the difference is due to plasmon emission pro-

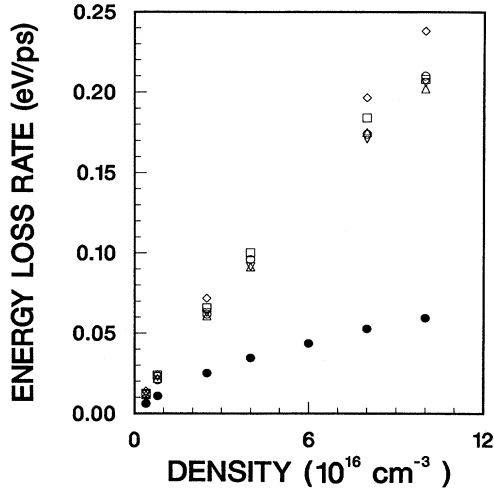


FIG. 3. Plots of the net energy-loss rate as a function of the plasma density. Dynamic-screening calculations are shown for a 300-meV hot electron, $T=100$ (square), 200 (circle), and 300 K (triangle); a 250-meV hot electron, 300 K (inverted triangle); a 200-meV hot electron, 100 K (diamond). Static-screening results are shown for a 300-meV hot electron and $T=100$ K (dot).

cesses that are not included in the SSA. Rota and Lugli¹⁶ have recently developed a Monte Carlo procedure for treating hot-electron-plasma scattering by *separately* including single-particle-like scattering events, using the SSA, and plasmon scattering events. This approach has the merit of computational simplicity, since the SSA results typically take an order of magnitude less time than the RPA calculations. In this context the self-consistent results shown in Fig. 3 can serve as a test for the accuracy of such non-self-consistent, but much simpler, approaches.

The other noteworthy feature of the results in Fig. 3 is the fact that the AELR due to plasma scattering is equal to the bare LO-phonon interaction rate, ~ 180 meV/ps, at $\sim 8 \times 10^{16} \text{ cm}^{-3}$. This result is relatively insensitive to the plasma temperature and the initial hot-electron energy. It therefore is one measure of the relative importance of plasma versus LO-phonon scattering, the conclusion being that plasma scattering starts to dominate above $\sim 8 \times 10^{16} \text{ cm}^{-3}$. This dominance is compounded due to the fact that the small wave-vector LO-phonon interactions are effectively screened at higher densities, as was shown in Fig. 2.

C. The total scattering rate

Integration of Eq. (9) without the multiplicative $\hbar\omega$ term results in the total scattering rate Γ of the hot electron out of its initial state:

$$\Gamma(\mathbf{k}) = \int_0^\infty dq \int_{-(\hbar q/2m)(2k+q)}^{(\hbar q/2m)(2k-q)} d\omega \frac{\partial^2 \Gamma(\mathbf{k})}{\partial \omega \partial q} [1 - f(\mathbf{k}-\mathbf{q})]. \quad (10)$$

In the limit that the kinetic energy of the hot electron is much larger than the temperature or Fermi level of the plasma (i.e., no significant scattering occurs from the plasma into this state), this TSR is identical to the imagi-

nary part of the hot-electron self-energy, within the RPA.⁴

Table I summarizes the TSR calculated from Eq. (10) using the SSA, the RPA with the lattice polarizability omitted, and the full RPA. Selected values are given at three different plasma temperatures and three initial hot-electron energies. There is a relatively strong dependence of the TSR on plasma temperature, and a weaker dependence on the initial hot-electron energy. This is consistent with what others have reported for the TSR due to electron-only plasmas.^{4,17} Only a single value is given for each of these parameters because the TSR turns out to be *essentially independent of the plasma density*, within $\sim 10\%$, over a range of densities from 4×10^{15} to 10^{17} cm^{-3} .

This somewhat surprising result can be analytically traced using a simplified plasmon-pole approximation for an $\epsilon(\omega)$ corresponding to a single-component plasma. In this case,

$$\epsilon_\infty \epsilon^{-1}(\omega) \sim 1 + \frac{\omega_p^2}{\omega^2 - \omega_p^2}, \quad (11)$$

where ω_p is the plasmon frequency, $\propto N^{1/2}$. The result for Γ follows immediately from Eq. (1):

$$\Gamma = \frac{e^2 m_e}{\hbar^2 k \epsilon_\infty} \omega_p [2N_B(\omega_p) + 1] \ln \left[\frac{2\hbar k^2}{m_e \omega_p} \right], \quad (12)$$

where N_B is the Bose-Einstein population factor. In the low-density limit, this population factor goes as $1/\beta\hbar\omega_p$, which cancels the density dependence in the residue of $\text{Im}[1/\epsilon(\omega)]$. At higher densities the population factor goes as unity, and there remains a power-law dependence to Γ .

Physically, the density independence of Γ implies that within the RPA, the reduction in scattering strength at lower densities exactly cancels the reduced probability of encountering an electron in the plasma. Further insight can be gained by studying the differential scattering rate $\partial\Gamma/\partial\omega$ obtained by carrying out only the q integration in Eq. (10). Representative spectra are shown in Fig. 4 for three different carrier densities. As the density decreases,

TABLE I. Total scattering rates (ps^{-1}) at plasma temperatures of 100, 200, and 300 K and initial hot-electron energies of 200, 250, and 300 meV. Values in the table were obtained using the static-screening approximation (()), the RPA approximation neglecting the lattice polarizability ({ }), and the full RPA, including the lattice polarizability ({}), where the bare phonon rate was subtracted.

$E(k)$ (meV)	T (K)		
	100	200	300
200	(2.4)	(5.2)	(7.9)
	[12]	[20]	[26]
250	(2.3)	(4.7)	(6.9)
			[25]
300	(2.1)	(4.2)	(6.2)
	[11]	[18]	[23]
	{9}	{15}	

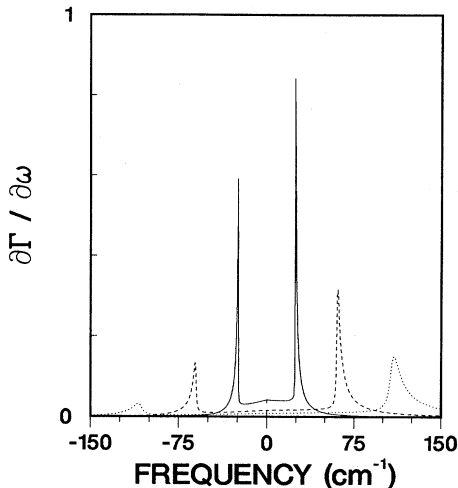


FIG. 4. The differential scattering rate for a 300-meV hot electron, $\partial\Gamma/\partial\omega$, obtained using the RPA without the lattice contribution ϵ_L , at $T=100$ K, and neutral plasma densities of 8×10^{16} (dot), 2.5×10^{16} (dash), and 4×10^{15} cm^{-3} (solid). The vertical scale has arbitrary units.

the area under the curves remains essentially constant, while the characteristic energy exchanged in either Stokes or anti-Stokes scattering processes decreases. There is also a relative increase in the importance of single-particle-like (nonresonant) scattering processes over plasmon (resonant) processes at lower densities. As the density decreases, the hot electron feels the effect of other carriers at larger separations and responds almost adiabatically by changing its energy and momentum only slightly, but still frequently.

All of these results beg the question of whether or not this TSR can be measured, in particular at low densities. (Note that the absolute value of the TSR due to the plasma is *larger* than that due to the bare LO-phonon interaction, even at extremely low densities.) An equally valid question is whether, despite the fact that the usual weakly coupled plasma criterion for the validity of the RPA is satisfied for this range of plasma parameters, the RPA is a valid approximation for calculating the self-energy of the hot electron under these low-density conditions. With respect to the former question, some type of coherence or dephasing experiment would be required that is sensitive to the quantum state lifetime of a hot electron in a state \mathbf{k} . A coherent interband optical measurement that couples the valence and conduction bands at \mathbf{k} is in principle sensitive to this state lifetime, in addition to the corresponding lifetime of the valence-band state. Böhne *et al.*¹⁸ have recently reported a theoretical model for such an experiment. Their expression for the measured dephasing rate (their Eq. 6.9) is the sum of two terms; the first is essentially equal to our Γ , and the second corresponds to vertex corrections. Böhne *et al.*¹⁸ comment on (without explicit derivation) the apparent unphysical density (in)dependence of the term if calculated within the RPA. They argue that the second term associated with vertex corrections will cancel Γ at low densities, in keeping with the intuitive result. If this is in fact the correct interpretation, then it is likely that Γ cannot

in fact be directly measured, in which case the relevance of our result is that it is one of the terms that must be calculated in modeling dephasing measurements, and any future calculations of the vertex corrections must cancel our result at low density.

In light of these properties of the TSR, revealed by studying their dependence on *carrier density*, care should perhaps be exercised in interpreting the relevance of detailed plasma temperature and hot-electron energy dependences of calculated TSR's.^{3,4,17}

D. Comparison with experiment

Kash¹⁵ has reported a pump-and-probe hot luminescence experiment designed to determine the density dependence of hot-electron-plasma scattering in GaAs at densities below $\sim 10^{17}$ cm^{-3} . The plasma was injected by a picosecond pump pulse and allowed to thermalize for ~ 30 ps, at which time the temperature of the electrons and holes was ~ 100 K. The plasma density could be easily varied by varying the power in the pump pulse. A second, much weaker probe pulse then injected a very low density of ~ 300 -meV electrons into the conduction band. The relaxation behavior of these as-injected hot electrons was then inferred by monitoring the luminescence emitted as a small fraction of the hot electrons recombined with neutral acceptors before scattering out of conduction-band states within the luminescence linewidth, ~ 20 meV full width at half maximum (FWHM). The integrated area under this as-excited luminescence feature is proportional to the average (in an ensemble sense) time that the as-excited electron remains in states that are within the measured linewidth of the as-excited states. With no pump pulse present, i.e., in the absence of a plasma, this time is expected to be determined by the LO-phonon scattering rate, ~ 5 ps^{-1} . In the presence of the plasma, Kash observed that the integrated luminescence decreased linearly with density, and was half as strong as with no plasma at a density of $\sim 8 \times 10^{16}$ cm^{-3} . He thus deduced that the hot-electron-plasma "scattering rate" was linearly proportional to the plasma density and became equal to the bare LO-phonon scattering rate at a density of $\sim 8 \times 10^{16}$ cm^{-3} .

To compare the calculated electron-plasma scattering rate with the results of this experiment, it is important to recognize that the experiment does not directly measure either the TSR, or the AELR. The TSR is a property of a single as-excited state, whereas the experiment is insensitive to scattering events that take the carrier out of the as-excited state, but leave it either directly or after multiple-scattering events, in states within the *set of states* that give rise to the relatively broad luminescence feature being measured. Thus the experimentally determined "scattering rate" will always be less than or equal to the TSR as calculated above.

The experiment also does not in general provide a measure of the AELR. In the hypothetical case that *all* of the scattering with the plasma occurred via well-defined plasmon modes (i.e., at a well-defined energy similar to LO-phonon scattering) and if the plasmon energy was

greater than the luminescence linewidth and larger than the thermal energy (i.e., no appreciable anti-Stokes scattering), then the experiment *would* measure the TSR. In this case the energy of the plasmon, so long as it is enough to take the carrier out of the luminescence linewidth, is irrelevant, and so therefore would be the AELR.

Thus, in general, the experimentally deduced “scattering rate” cannot be simply related to either the TSR or the AELR. One way to model the results is by using the differential scattering rate $\partial\Gamma/\partial\omega$ in an ensemble simulation of the actual experimental conditions. Specifically, starting with the hot electron in the as-excited state (assumed to be in the center of the luminescence spectrum), scattering events are allowed to occur at random, but on average at a rate determined by the TSR. The final state of each scattering event is determined from $\partial\Gamma/\partial\omega$, and the simulation is allowed to continue until the electron effectively never reenters states with energy within the luminescence linewidth of the as-excited state. The inverse of an ensemble average of the time over which electrons remained within this range of states was then compared with the experimental “scattering rate,” as shown in Fig. 5. These simulations were carried out separately using (i) the RPA and the full $\epsilon(\omega, \mathbf{q})$ (in which case the bare LO-phonon contribution was subtracted off), (ii) the RPA omitting the lattice contribution $\epsilon_L(\omega)$ from $\epsilon(\omega, \mathbf{q})$, and (iii) the SSA. Note that, with no adjustable parameters, the result obtained from these simulations agrees very well with the experimentally determined result¹⁵ provided the full $\epsilon(\omega, \mathbf{q})$ is used. Within the experimental and numerical errors, the RPA result obtained by omitting the lattice contribution is also in agreement, but

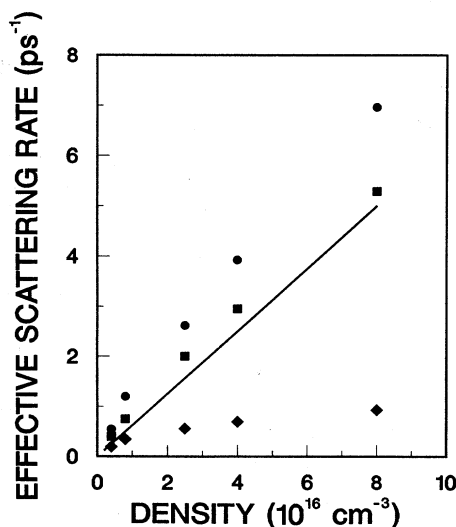


FIG. 5. Plots of the “effective” scattering rate out of an energy window 20 meV wide for a 300-meV hot electron interacting with a 100-K electron-hole plasma as a function of the plasma density. The different curves correspond to calculations using the static-screening approximation (diamonds), the RPA including the lattice polarizability (squares), and the RPA excluding the lattice polarizability (circles). The solid line represents the result as inferred from experiment (Ref. 15).

the results from the SSA do not reproduce the experimental results.

From the density independence of the TSR, the differential scattering rates shown in Fig. 4, and the AELR shown in Fig. 3, we can conclude that the “scattering rate” measured by Kash is more closely related to the AELR than it is to the TSR. In essence, at low densities the hot carrier is undergoing many small-angle, low-energy scattering events that contribute to the TSR but which tend to cancel in their contribution to net energy change (due to the large anti-Stokes–Stokes ratio at low energy). In addition, even ignoring the role of anti-Stokes processes, numerous individual scattering events are required to take the as-excited electron out of the luminescence linewidth at low densities.

IV. PARTITIONING OF THE ENERGY AMONG THE PLASMA COMPONENTS

The model used above was purposefully chosen to represent a physically realizable, yet close-to-equilibrium, system of interest that could be delicately probed without significantly altering the properties of the system. The quasiequilibrium (isothermal) assumption was required to avoid the highly nontrivial many-body complications^{19–21} that arise even when the various system components can still be characterized by effective, but different, temperatures. In the event that the hot electrons did not act as *weak* probes (i.e., if their density became comparable to that of the plasma), then it would be necessary to incorporate generalized versions of these scattering calculations with sets of kinetic equations in order to model accurately the overall system’s dynamics. Under such conditions, the temperatures of the electrons, holes, and phonons could no longer be assumed equal (in general they will be influenced by the energy transferred to them from the hot electrons), thus invalidating the quasiequilibrium approach.

The self-consistent many-body solution to this more general problem is well beyond the scope of the present investigation. However, one of the key issues that will have to be addressed in this context has to do with integrating these microscopic scattering equations with kinetic equations that keep account of how the energy is partitioned among the various system subcomponents. Towards this ultimate end, the relative coupling strength of the hot electrons to various subcomponents is an important parameter that can be addressed (in the limit of quasiequilibrium conditions) using the present model.

Within the SSA, the relative energy-transfer rate from the hot electrons to the various plasma subcomponents is unambiguously obtained by independently evaluating the contributions that each of the intraband and interband terms in the expansion of $\text{Im}[1/\epsilon(\omega, \mathbf{q})]$ [see Eq. (7)] makes to dE/dt in Eq. (9). Each term then directly represents the various ways in which energy is transferred through direct, single-particle-like transitions within or between bands. Figure 6 shows one example of the partitioning of the overall AELR into (i) intra-conduction band, (ii) intra-heavy and intra-light valence-band, and (iii) inter-heavy-to-light valence-band processes

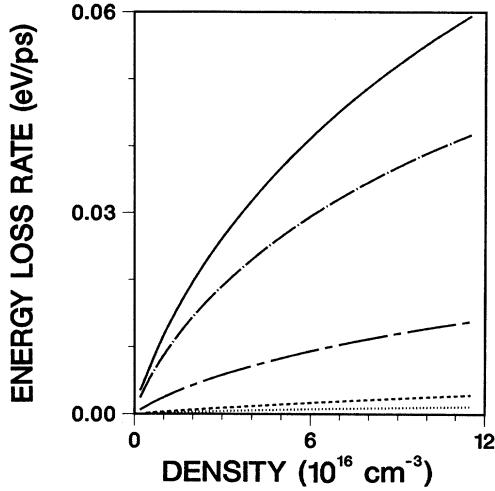


FIG. 6. The total energy-loss rate of a 300-meV hot electron in a neutral plasma as a function of density at $T=100$ K obtained with the static-screening (solid line) approximation. Separate contributions from intraband electrons (dot-dashed), heavy holes (dashed), light holes (dotted), and with the interband holes (short-dashed–long-dashed) are also shown.

for a 300-meV hot electron and a 300-K plasma. Analysis of similar plots for different plasma temperatures shows that energy transfer via conduction-band electrons is always the most efficient process. Intra-heavy- and intra-light-hole processes (classical Coulomb scattering events) typically account for $< 15\%$ of the total, due largely to the quasielastic nature of the light-electron–heavy-hole scattering and to the relatively low density of light holes. The inter-valence-band processes can, however, contribute close to 25% of the total AELR under certain conditions.

In the dynamically screened case, the contributions of various intraband and interband terms can still be separately evaluated in Eq. (9); however, the interpretation of the results is less clear than in the SSA. Figure 7 illustrates the various contributions to the integrand of Γ from different intraband and interband terms at a fixed plasma density of $8 \times 10^{16} \text{ cm}^{-3}$. It is clear that the intra-heavy-hole contribution [to be compared to Fig. 1(a)] is essentially the same as that obtained in the SSA. That the electron–heavy-hole scattering process need not be dynamically screened has been previously shown by Collet²² and by Sato and Hori,⁵ and it can be understood simply with reference to a schematic diagram of the collective and single-particle excitation spectra of the various plasma subcomponents (see Fig. 8, and note that this diagram, and the following arguments, are based on a zero-temperature situation; however, the qualitative features at issue apply more generally).

The energy and dispersion of the collective plasmon mode of the multicomponent plasma is dominated by the electrons due to their large number and small mass. The plasmon mode is a well-defined resonance only for relatively small wave vectors, below those at which it intersects the system’s single-particle excitation spectrum, at which point the plasmon suffers strong Landau damping.

Given the weak dispersion of the massive heavy-hole single-particle spectrum, there is essentially no overlap of well-defined plasmons and heavy-hole single-particle excitations; hence, there is no plasmon enhancement of the latter. The SSA therefore provides an accurate treatment of the hot-electron–heavy-hole scattering process.

Again with reference to Fig. 8, there does exist overlapping phase space for the plasmon with intra-conduction and intra-light-hole single-particle excitations (right where they merge, at the onset of Landau damping), and with inter-valence-band single-particle excitations. This explains the resonant peaks that appear for each of these processes in the differential scattering rates of Fig. 7. The various contributions in Fig. 7 reflect the relative coupling efficiency of the hot electron’s energy into the various subcomponents via scattering from corresponding, correlated charge-density fluctuations. This follows directly from the fluctuation-dissipation theorem that relates the linear-response function $\epsilon(\omega, q)$ to the density-density correlation function $T(\omega, \mathbf{q})$ (Ref. 10),

$$\begin{aligned} T(\omega, \mathbf{q}) &= \frac{1}{2\pi} \int_{-\infty}^{\infty} dt \langle n_{\mathbf{q}}(0) n_{-\mathbf{q}}(t) \rangle e^{i\omega t} \\ &= \frac{1}{V(q)} \frac{1}{(1 - e^{\beta\hbar\omega})} \text{Im} \left[\frac{1}{\epsilon(\omega, \mathbf{q})} \right]. \end{aligned} \quad (13)$$

There is a complication, however, when considering how to incorporate this information into a kinetic model. The energy transferred resonantly through the plasmon will be stored collectively for a time associated with the resonant width. In general, this storage time could be long compared to other relaxation processes, including the characteristic plasmon emission time itself. This is one specific example of the nontrivial many-body problems involved in going beyond the quasiequilibrium, weak-probe approximation. Qualitatively, it may be possible to design the kinetic model to include an independent “temperature” for plasmons, and hence account for the resonant storage; however, this would have to be done with care and verified with respect to a full nonequilibrium many-body treatment.

The above complications owing to resonant storage notwithstanding, it is of interest to determine the relative energy-transfer efficiencies for the hot electron via the various intraband and interband charge-density fluctuations. The ratio of the total-energy transfer rates via intra-conduction-band to all intra- and inter-valence-band processes (i.e., relative efficiency via electrons versus holes) is plotted in Fig. 9 for the same plasma parameters for which the AELR was shown in Fig. 3. Note that while there was very little dependence of the AELR on the plasma and hot-electron parameters, there is a very significant effect of these on the partitioning of the energy to the electron and hole subsystems. In particular, there are ranges of parameter space for which the energy transfer to the holes is comparable to that to the electrons, and other regions where the role of holes is negligible.

As can be inferred from Figs. 6 and 7, in circumstances where the holes make a large contribution, it is the inter-valence-band, rather than the intra-valence-band, pro-

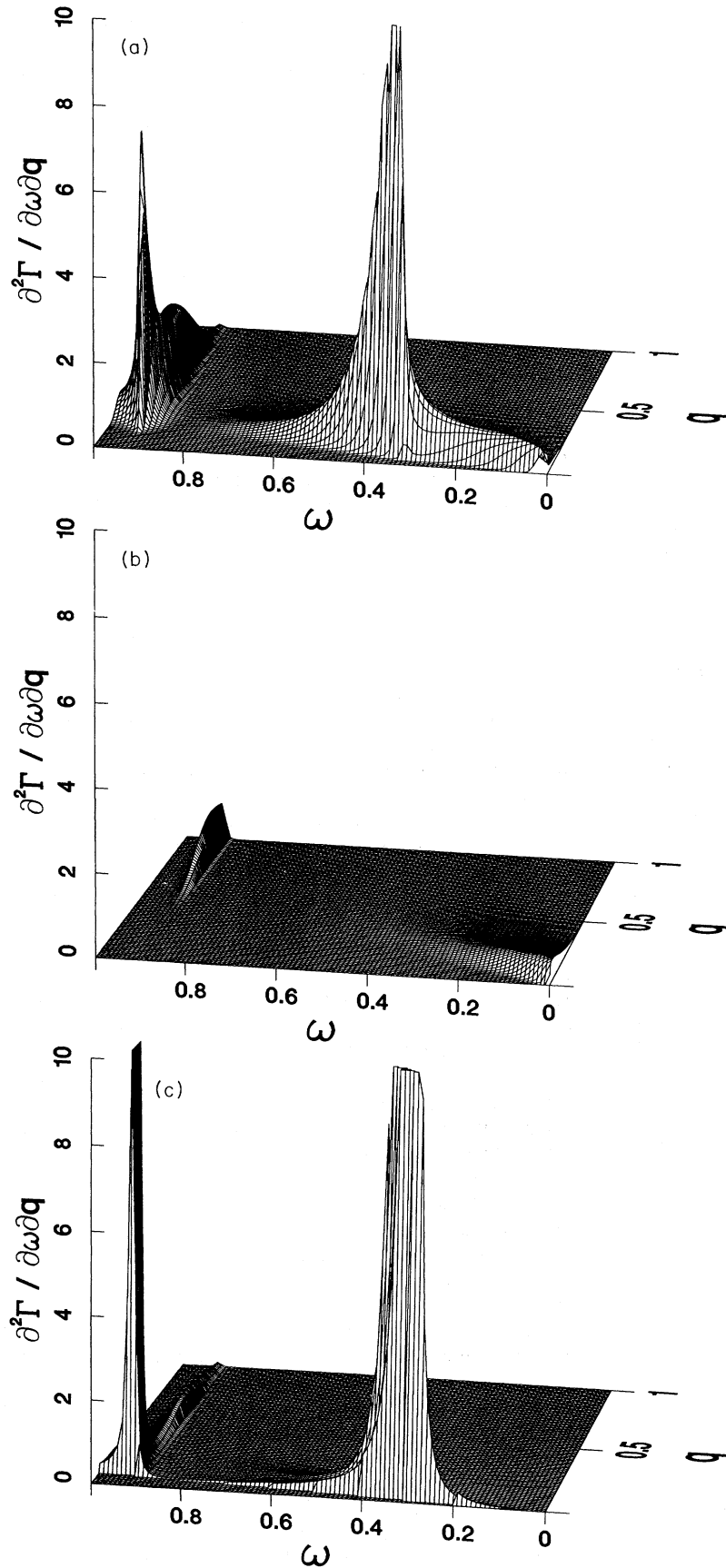


FIG. 7. Contributions to the integrand of Eq. (10) obtained using dynamic screening, including the lattice susceptibility due to (a) intra-conduction-band fluctuations, (b) intra-heavy-hole band fluctuations, and (c) inter-heavy-to-light-hole fluctuations. Full scale in wave vector corresponds to $5 \times 10^6 \text{ cm}^{-1}$, and full scale in frequency corresponds to $6 \times 10^{13} \text{ rad/s}$. The integrand is on the same vertical scale for (a), (b), and (c), and the absolute values can be compared directly with the integrands of Fig. 1.

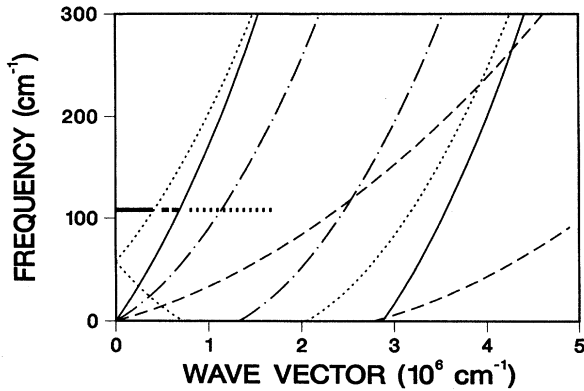


FIG. 8. A schematic representation of the single-particle and collective mode excitation spectra of the neutral plasma at a density of $\sim 1 \times 10^{17} \text{ cm}^{-3}$ and zero temperature. The regions where single-particle excitations are allowed correspond to the areas enclosed by (i) solid curves (electrons), (ii) dashed curves (heavy holes), (iii) dash-dotted curves (light holes), and (iv) dotted curves (inter-heavy-to-light hole). The straight line schematically illustrates the collective plasmon excitation spectrum (neglecting dispersion), with decreasing line density representing increasing damping.

cesses that dominate. Qualitatively, this can be understood with reference again to Fig. 8, since the inter-valence-band single-particle excitation spectrum is quite different than that of the intra-valence-band processes, and there can be a large overlap of the plasmon and inter-valence-band phase spaces. *Quantitatively*, the relative importance of electrons and holes can be understood over quite a large range of plasma and hot-electron parameter space by deriving appropriate scaling factors for the two axes in Fig. 9. Thus, by normalizing the ratio R on the ordinate of Fig. 9 by

$$\eta_1 = k' \sqrt{\beta'} \quad (14)$$

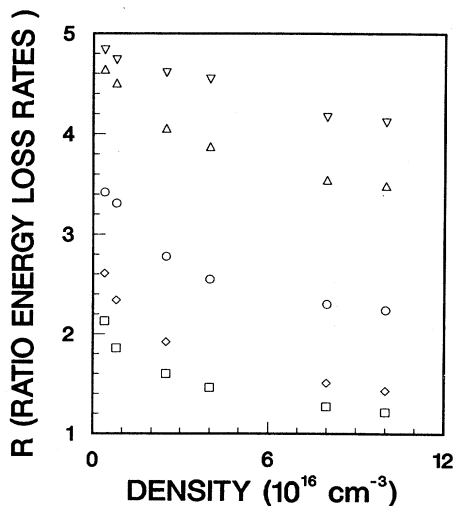


FIG. 9. Ratios R of the net energy-loss rate via electrons to that via holes as a function of plasma density for the same sets of RPA parameters (symbols) as in Fig. 3.

and plotting this against

$$\eta_2 = \frac{e^\xi}{\xi}, \quad (15)$$

where

$$\xi = \frac{\beta \hbar \omega_p}{\frac{m_h}{m_l} - 1}, \quad (16)$$

it is possible to reduce the data in Fig. 9 to a “universal” curve, as shown in Fig. 10. The primes in Eq. (14) indicate that k and β are normalized using the GaAs exciton Böhr radius ($\sim 100 \text{ \AA}$) and binding energy ($\sim 6.6 \text{ meV}$), respectively.

With reference to Eq. (1), the derivation of the normalization factor η_1 can be traced to evaluating the $1/q$ term associated with the plasmon-enhanced intra-electron and inter-valence-band processes. From the plots in Fig. 7, the resonant enhancements for both intra-conduction-band and inter-valence-band terms occur at quite well-defined, and different, values of q . The characteristic q , $q = q_v$ for the inter-valence-band process, is easy to derive; it occurs at the smallest kinematically allowed q value for plasmon interaction, or where

$$\hbar \omega_p \approx \frac{\hbar^2 k q_v}{m_e} = q_v \sim \frac{m_e \omega_p}{\hbar k}. \quad (17)$$

The characteristic q , $q = q_e$, for intra-conduction-band processes, is more difficult to obtain, but can be derived approximately by resorting to a single-component, classical expression for $\epsilon(\omega, q)$, which in the limit of $\beta m_e \omega^2 / q^2 \gg 1$, is

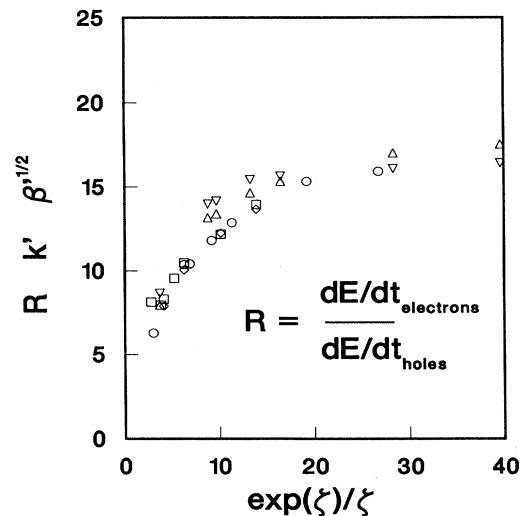


FIG. 10. A scaled version of the plot in Fig. 9 illustrating the dependence of the *normalized* R on the *normalized* plasma density. The normalization parameters are discussed in detail in the text.

$$\epsilon(\omega, q) \sim \epsilon_\infty \left[1 - \frac{\omega_p^2}{\omega^2} \left[\left\{ 1 + \frac{3}{2} \frac{x}{\omega^2} \right\} - i \left(\frac{\pi}{2} \right)^{1/2} \left(\frac{2\omega^2}{x} \right)^{3/2} e^{\omega^2/x} \right] \right], \quad (18)$$

where $x = 2q^2/\beta m_e$. It is then possible to determine analytically the q value at which the integrand of Eq. (9) is a maximum. The resulting secular equation is a function only of x/ω_p^2 , so that the maximum contribution near ω_p is given approximately by

$$\frac{x}{\omega_p^2} = C \implies q_c \simeq \frac{1}{\sqrt{\beta}} \left[\frac{m_e C}{2} \right]^{1/2} \beta \omega_p, \quad (19)$$

where C is a constant, ~ 0.2 , in GaAs. The η_1 normalization factor, Eq. (14), is then just proportional to q_c/q_v .

The scaling factor for the abscissa comes from estimating the contribution to Eq. (9) from the $\text{Im}[1/\epsilon(\omega, \mathbf{q})]$ term, assuming all of the weight occurs at the plasmon frequency, for both intra-conduction-band and inter-valence-band processes. This can be reduced to estimating the relative plasmon-related transition rates for the two processes, which are independently proportional to the product of the density of initial and final states available for the transitions, multiplied by a Boltzmann population factor for the occupation of the initial states. For the inter-valence-band process, if the small but nonzero wave vector derived in Eq. (17) is neglected, then vertical transitions from the heavy-hole band to the light-hole band occur at a wave vector k_{int} of

$$k_{\text{int}}^2 \simeq \frac{2m_l m_h}{m_h - m_l} \frac{\omega_p}{\hbar}. \quad (20)$$

The product of the initial and final density of states, and the Boltzmann population factor for the initial heavy-hole states, T_{int} at k_{int} is then proportional to

$$T_{\text{int}} \propto \frac{\hbar \omega_p}{m_h - m_l} (m_l m_h)^{1/2} e^{-\beta \hbar \omega_p m_l / (m_h - m_l)}. \quad (21)$$

Following the same procedure for the intra-conduction-band contribution and using the value of q_c derived above to determine the initial states k_e from which the majority of the plasmon transitions occur, then, in the limit of small $\beta \hbar \omega_p$,

$$\frac{\hbar^2 k_e^2}{2m_e} \simeq \frac{1}{\sqrt{2C} \beta}, \quad (22)$$

and the corresponding transition rate T_{ee} is proportional to

$$T_{ee} \propto \frac{1}{\sqrt{2C} \beta} e^{-1/\sqrt{2C}}. \quad (23)$$

The ratio of T_{ee} and T_{int} is thus proportional to the scaling factor η_2 in Eq. (15).

Together, the information in Figs. 3 and 10 provides quite general, dynamically screened results that should be useful for simply estimating both the AELR and its partitioning between conduction-band and valence-band carriers.

V. CONCLUSIONS

The scattering of a hot (~ 200 – 300 meV) “test” electron with neutral electron-hole plasmas in GaAs has been studied within the Born approximation using both static- and dynamic- (exact within the random-phase approximation) screening calculations. Although numerical results are presented only for GaAs, the general formalism is applicable to other zinc-blende semiconductors. Both approximations yield a total scattering rate (out of a fixed initial momentum state) that is nearly independent of plasma density over a wide range of densities from 10^{15} to 10^{17} cm^{-3} , but which is quite sensitive to the plasma temperature and the energy of the test electron. This total scattering rate is a contributing factor to the dephasing rate that coherent interband optical experiments (in the presence of a neutral plasma) measure, although other processes may also contribute to specific experimentally determined scattering rates. Total scattering rates obtained using the static-screening approximation are typically a factor of 5 to 10 less than those obtained using full dynamic screening.

In contrast to the total scattering rate, the average (in an ensemble sense) energy-loss rate of the test electron is found to be quite insensitive to the plasma temperature and the initial hot-electron energy. This energy-loss rate is almost linearly dependent on plasma density when dynamic screening is used, but exhibits a sublinear density dependence within the static-screening approximation. The partitioning of energy lost by the hot electron to the electron and hole components of the plasma was found to be sensitive to the plasma temperature and hot-electron energy. Under certain conditions, almost as much energy is transferred to the holes as to the electrons, but the electrons typically absorb most of the energy. By recognizing that significant amounts of energy get transferred to the holes only via inter-heavy-to-light valence-band processes resonantly enhanced by collective plasma oscillations, scaling factors were derived that can be used to factor out the plasma temperature and hot-electron-energy dependence to the partitioning of energy to electrons versus holes. This means that dynamically screened calculations of both the net energy-loss rate and its partitioning between electron and hole subsystems can be easily obtained over a wide range of plasma and hot-electron parameter space by simple reference to two “universal” curves.

Finally, quantitative agreement with hot-electron-plasma scattering experiments by Kash¹⁵ was obtained using the dynamically screened scattering rates

together with a simple one-dimensional Monte Carlo routine. The statically screened calculations always underestimated the experimental results, which exhibit a linear density dependence and become equal to the bare LO-phonon scattering rate of $\sim 5 \text{ ps}^{-1}$ at a density of $\sim 8 \times 10^{16} \text{ cm}^{-3}$.

ACKNOWLEDGMENTS

We thank Norm L. Henry for his help in initiating this project and Dr. Agnes Hsu for computational support.

We also readily thank Dr. Chandre Dharma-wardana and Dr. Pawel Hawrylak for many useful learning sessions.

APPENDIX: THE RPA DIELECTRIC FUNCTION

1. Intraband terms

Using Eq. (6) in Eq. (5) with a change of variable in the second population factor, the general intraband term can be written

$$\text{Im}\{P^{ii}(\omega, \mathbf{q})\} = \frac{1}{(2\pi)^2} \int d\mathbf{k} f^i(\mathbf{k}) \frac{1}{4} \left\{ 1 + \frac{3(k^2 + \mathbf{q} \cdot \mathbf{k})^2}{k^2(q^2 + k^2 + 2\mathbf{q} \cdot \mathbf{k})} \right\} \{ \delta(\hbar\omega - E_{\mathbf{k}} + E_{\mathbf{k}+\mathbf{q}}) - \delta(\hbar\omega - E_{\mathbf{k}+\mathbf{q}} + E_{\mathbf{k}}) \}. \quad (\text{A1})$$

Reexpressing the δ functions as

$$\begin{aligned} \delta(\hbar\omega - E_{\mathbf{k}} + E_{\mathbf{k}+\mathbf{q}}) &= \frac{m_i}{\hbar^2 k q} \delta \left[\cos\theta - \frac{S_-}{kq} \right], \\ \delta(\hbar\omega + E_{\mathbf{k}} - E_{\mathbf{k}+\mathbf{q}}) &= \frac{m_i}{\hbar^2 k q} \delta \left[\cos\theta - \frac{S_+}{kq} \right], \end{aligned} \quad (\text{A2})$$

where

$$S_{\pm} \equiv \pm \frac{m_i \omega}{\hbar} - \frac{q^2}{2},$$

the integration can be explicitly written as

$$\begin{aligned} \text{Im}\{P^{ii}(\omega, \mathbf{q})\} &= \frac{m_i}{2\pi\hbar^2 q} \left[\int_{|S_-|/q}^{\infty} dk k f^i(k) \frac{1}{4} \left\{ 1 + \frac{3(k^2 + S_-)^2}{k^2(q^2 + k^2 + 2S_-)} \right\} \right. \\ &\quad \left. - \int_{|S_+|/q}^{\infty} dk k f^i(k) \frac{1}{4} \left\{ 1 + \frac{3(k^2 + S_+)^2}{k^2(q^2 + k^2 + 2S_+)} \right\} \right]. \end{aligned} \quad (\text{A3})$$

Assuming Maxwell-Boltzmann population factors f ,

$$\text{Im}\{P^{ii}(\omega, \mathbf{q})\} = \frac{m_i n}{4\pi\hbar^2 q \alpha_i} \left[\int_{\alpha_i S_-^2 / q^2}^{\infty} dt e^{-t} \frac{1}{4} \left\{ 1 + \frac{3(t + \alpha_i S_-)^2}{t(t-b)} \right\} - \int_{\alpha_i S_+^2 / q^2}^{\infty} dt e^{-t} \frac{1}{4} \left\{ 1 + \frac{3(t + \alpha_i S_+)^2}{t(t+b)} \right\} \right], \quad (\text{A4})$$

where

$$b \equiv \frac{2m_i \alpha_i \omega}{\hbar}, \quad \alpha_i \equiv \frac{\hbar^2}{2m_i} \left[\frac{1}{k_B T} \right], \quad \text{and } n = 4(\pi\alpha_h)^{3/2} (N_h + N_l) / \left[1 + \left(\frac{m_l}{m_h} \right)^{3/2} \right].$$

Finally, with $E_1(x)$, the exponential integral²³ of x , then the hole intraband terms can be expressed as

$$\begin{aligned} \text{Im}\{P^{ii}(\omega, \mathbf{q})\} &= \frac{m_i n}{16\pi\hbar^2 q \alpha_i} \left\{ 4 \left[e^{-(\alpha_i S_-^2 / q^2)} - e^{-(\alpha_i S_+^2 / q^2)} \right] \right. \\ &\quad \left. + \frac{3\alpha_i^2}{b} \left[(e^{-b} - 1) S_+^2 E_1 \left[\frac{\alpha_i S_+^2}{q^2} \right] + (e^b - 1) S_-^2 E_1 \left[\frac{\alpha_i S_-^2}{q^2} \right] \right] \right\}. \end{aligned} \quad (\text{A5})$$

Taking the matrix element equal to unity and treating the electrons with Fermi-Dirac statistics, the well-known electron intraband polarizability results from Eq. (A3):

$$\text{Im}\{P^{ee}(\omega, \mathbf{q})\} = \frac{m_e}{4\pi\hbar^2 q} \ln \left[\frac{1 + e^{-(\alpha_e S_-^2 / q^2) + \eta}}{1 + e^{-(\alpha_e S_+^2 / q^2) + \eta}} \right], \quad (\text{A6})$$

where $\eta = \beta\mu_e$ and μ_e is the electron chemical potential, which is known, given T and N_e .

2. Interband terms

Similar to Eq. (A1), the general interband term can be written

$$\begin{aligned} \text{Im}\{P^{ij}(\omega, \mathbf{q})\} &= \frac{1}{(2\pi)^2} \int d\mathbf{k} f^i(\mathbf{k}) \frac{3}{4} \left\{ 1 - \frac{(k^2 + \mathbf{q} \cdot \mathbf{k})^2}{k^2(q^2 + k^2 + 2\mathbf{q} \cdot \mathbf{k})} \right\} \\ &\quad \times \{ \delta(\hbar\omega - E_{\mathbf{k}}^i + E_{\mathbf{k}+\mathbf{q}}^f) \\ &\quad - \delta(\hbar\omega + E_{\mathbf{k}}^i - E_{\mathbf{k}+\mathbf{q}}^f) \}. \end{aligned} \quad (\text{A7})$$

The δ functions, in turn, can be written as

$$\delta(\hbar\omega \mp E_{\mathbf{k}}^i \pm E_{\mathbf{k}+\mathbf{q}}^f) = \frac{m_f}{\hbar^2 k q} \delta \left[\cos\theta \left[\frac{T_{\mp}}{kq} + \frac{a}{q} k \right] \right], \quad (\text{A8})$$

where

$$a \equiv \frac{1}{2} \left[\frac{m_f}{m_i} - 1 \right] \quad \text{and} \quad T_{\pm} \equiv \pm \frac{m_f \omega}{\hbar} - \frac{q^2}{2}.$$

Since the limits of integration are given by the δ -function integration as

$$-1 \leq \frac{T_-}{kq} + \frac{a}{q} k \leq 1 \quad \text{and} \quad -1 \leq \frac{T_+}{kq} + \frac{a}{q} k \leq 1,$$

we split the interband term up into the two parts because of the sign dependence of a :

$$\text{Im}\{P^{lh}(\omega, \mathbf{q})\} = \begin{cases} I_- - I_+, & 0 \leq \hbar\omega \leq E_q \\ I_-, & \hbar\omega > E_q, \end{cases} \quad (\text{A9})$$

$$\text{Im}\{P^{hl}(\omega, \mathbf{q})\} = \begin{cases} I_- - I_+, & 0 \leq \hbar\omega \leq E_q \\ -I_+, & \hbar\omega > E_q, \end{cases} \quad (\text{A10})$$

where

$$E_q = \hbar^2 q^2 / 2(m_h - m_l),$$

and

$$\begin{aligned} I_- &\equiv \frac{m_f}{2\pi\hbar^2 q} \int_{|Q_-|}^{|Q_+|} dk k f^i(k) \frac{3}{4} \left\{ 1 - \frac{[k^2(1+a) + T_-]^2}{k^2[k^2(1+2a) + q^2 + 2T_-]} \right\}, \\ I_+ &\equiv \frac{m_f}{2\pi\hbar^2 q} \int_{|R_-|}^{|R_+|} dk k f^i(k) \frac{3}{4} \left\{ 1 - \frac{[k^2(1+a) + T_+]^2}{k^2[k^2(1+2a) + q^2 + 2T_+]} \right\}, \end{aligned}$$

and

$$\begin{aligned} Q_{\pm} &\equiv \frac{q}{2a} \left\{ 1 \pm \left[1 - \frac{4T_- a}{q^2} \right]^{1/2} \right\}, \\ R_{\pm} &\equiv \frac{q}{2a} \left\{ 1 \pm \left[1 - \frac{4T_+ a}{q^2} \right]^{1/2} \right\}. \end{aligned} \quad (\text{A11})$$

Again using Maxwell-Boltzmann population factors and some tedious algebra,

$$\begin{aligned} I_- &= \frac{3m_f n}{16\pi\hbar^2 q \alpha_i} \left\{ -\frac{(m_f - m_i)^2}{4m_f m_i} [e^{-(\alpha_i Q_-^2)} - e^{-(\alpha_i Q_+^2)}] - \frac{m_i \alpha_i^2}{m_f b} [S_+^2 e^{-b} \{E_1(\alpha_i Q_-^2 - b) - E_1(\alpha_i Q_+^2 - b)\}] \right. \\ &\quad \left. - T_-^2 \{E_1(\alpha_i Q_-^2) - E_1(\alpha_i Q_+^2)\} \right\}, \end{aligned} \quad (\text{A12})$$

$$\begin{aligned} I_+ &= \frac{3m_f n}{16\pi\hbar^2 q \alpha_i} \left\{ -\frac{(m_f - m_i)^2}{4m_f m_i} [e^{-(\alpha_i R_-^2)} - e^{-(\alpha_i R_+^2)}] - \frac{m_i \alpha_i^2}{m_f b} [S_-^2 e^b \{E_1(\alpha_i R_-^2 + b) - E_1(\alpha_i R_+^2 + b)\}] \right. \\ &\quad \left. - T_+^2 \{E_1(\alpha_i R_-^2) - E_1(\alpha_i R_+^2)\} \right\}. \end{aligned} \quad (\text{A13})$$

3. Numerical procedure

Throughout, we have considered GaAs band parameters. The effective masses of electrons, heavy holes, and light holes were taken as 0.067, 0.45, and 0.82, respectively. The high- and low-frequency dielectric constants ϵ_{∞} and ϵ_0 were taken as 10.92 and 12.94, respectively. For

electron densities $\leq 10^{18} \text{ cm}^{-3}$ and $100 \leq T_e \leq 300 \text{ K}$, the complete analysis can be done with Maxwell-Boltzmann statistics with the estimate of error in our work about 10% provided $dE/dt \geq 1 \text{ meV/ps}$ or $\Gamma \geq 1 \text{ ps}^{-1}$. A good test of our integration procedure is that we obtain $dE/dt \approx 180 \text{ meV/ps}$ due to the phonon peak when $N_e \approx 10^{15} \text{ cm}^{-3}$.

- ¹J. A. Kash, J. C. Tsang, and J. M. Hvam, *Phys. Rev. Lett.* **54**, 2151 (1985).
- ²S. Zollner, S. Gopalan, and M. Cardona, *Solid State Commun.* **76**, 877 (1990).
- ³A. F. J. Levi and Y. Yafet, *Appl. Phys. Lett.* **51**, 42 (1987).
- ⁴J. M. Rorison and D. C. Herbert, *J. Phys. C* **19**, 3991 (1986).
- ⁵H. Sato and Y. Hori, *Phys. Rev. B* **36**, 6033 (1987).
- ⁶D. Yevick and W. Bardyszewski, *Phys. Rev. B* **39**, 8605 (1989).
- ⁷J. F. Young, N. L. Henry, and P. J. Kelly, *Solid-State Electron.* **32**, 1567 (1989).
- ⁸J. F. Young, P. J. Kelly, N. L. Henry, and M. W. C. Dharma-wardana, *Solid State Commun.* **78**, 343 (1991).
- ⁹J. F. Young, P. J. Kelly, and N. L. Henry, *Semicond. Sci. Technol.* **B 7**, 148 (1992).
- ¹⁰P. M. Platzman and P. A. Wolff, *Waves and Interactions in Solid State Physics* (Academic, New York, 1973), Suppl. 13.
- ¹¹G. D. Mahan, *Many-Particle Physics* (Plenum, New York, 1981).
- ¹²J. M. Ziman, *Principles of the Theory of Solids* (Cambridge University Press, Cambridge, 1972).
- ¹³M. Combescot and P. Nozières, *J. Phys. C* **5**, 2369 (1972).
- ¹⁴We note that obtaining the correct bare phonon result by integrating the phonon peak at low densities provides a good test for the accuracy of the numerical integration scheme.
- ¹⁵J. A. Kash, *Phys. Rev. B* **40**, 3455 (1989).
- ¹⁶L. Rota and P. Lugli, *Semicond. Sci. Technol.* **B 7**, 180 (1992).
- ¹⁷B. Y. K. Hu and S. Das Sarma, *Phys. Rev. B* **44**, 8319 (1991).
- ¹⁸G. Böhne, T. Sure, R. G. Ulbrich, and W. Schäfer, *Phys. Rev. B* **41**, 7549 (1987).
- ¹⁹J. K. Jain, R. Jalabert, and S. Das Sarma, *Phys. Rev. Lett.* **60**, 353 (1988).
- ²⁰M. W. C. Dharma-wardana, *Phys. Rev. Lett.* **66**, 197 (1991).
- ²¹S. Das Sarma and V. Korenman, *Phys. Rev. Lett.* **67**, 2916 (1991); M. W. C. Dharma-wardana, *ibid.* **67**, 2917 (1991).
- ²²J. H. Collet, *Phys. Rev. B* **39**, 7659 (1989).
- ²³M. Abramowitz and I. A. Stegun, *Handbook of Mathematical Functions* (Dover, New York, 1970).